XIV International Conference on Computational Plasticity. Fundamentals and Applications
COMPLAS XIV
E. Oñate, D.R.J. Owen, D. Peric & M. Chiumenti (Eds)

ANALYSIS OF DAMAGE AND FRACTURE FORMULATIONS IN COLD EXTRUSION

ALEXANDER SCHOWTJAK*, TILL CLAUSMEYER* AND A. ERMAN TEKKAYA*

*Institute of Forming Technology and Lightweight Components (IUL)
Department of Mechanical Engineering, Technical University Dortmund
Baroper Str. 303, 44227 Dortmund, Germany
e-mail: Alexander.Schowtjak@iul.tu-dortmund.de, web page: http://www.iul.eu

Key words: Forming Processes, Finite Element Method, Plasticity, Damage, Fracture, Parameter Identification

Abstract. In forming processes, components generally undergo large deformations. This induces the evolution of damage, which can influence material and product properties. To capture these effects, a continuum damage mechanics (CDM) model, based on the work of Lemaitre [8] and Soyarslan [13, 14] as well as different fracture criteria according to Cockcroft and Latham [2], Freudenthal [4] and Oyane [10] are implemented and investigated. While the CDM theory considers the evolution of damage and the associated softening, fracture criteria do not affect the results of the mechanical finite element (FE) analysis. However, a coupling is generally possible via element deletion, but material softening cannot be depicted in the simulation. Tensile tests with notched specimens are performed in order to obtain the material parameters associated with these models by inverse parameter identification processes. The optimized set of parameters is finally applied to the damage and fracture models used for the FE simulations of a cold extrusion process, which are investigated in terms of damage evolution and material failure. It is demonstrated that the CDM model predicts the evolution of damage observed for different process parameters in cold extrusion quantitatively. The prediction of the failure by the fracture criteria does not agree well with the experiments.

1 INTRODUCTION

In forming processes, the material used to produce components generally undergo large deformations. For metals, this implies large plastic strains and damage, which has a significant effect on the material, and thus, product properties. The depiction of damage in FE-simulations is therefore necessary.

On the microscopic scale, damage occurs at inhomogenities such as inclusions or grain boundaries. During deformation, damage develops as a result of nucleation, growth and coalescence of voids. Excessive growth of these voids finally leads to macroscopic cracks,

and thus, failure of the component. The mere existence of damage, however, does not necessarily imply failure of the part, as Tekkaya et al. point out in [16].

The prediction of damage and fracture with finite element (FE) simulations requires the definition of a constitutive damage model to properly depict the physical behavior. McVeigh et al. [9], Saanouni et al. [12] and Soyarslan et al. [13] investigated cold extrusion processes by predicting central bursting in FE analyses with the use of continuum damage mechanics (CDM) theory. McVeigh et al. implemented a combined Drucker-Prager/HLC-type yield surface based on a micromechanical cell modeling technique. Soyarslan et al. performed investigations based on a Lemaitre-type damage model with fictitious material parameters, while Saanouni et al. used parameters which were identified based solely on uniaxial tensile tests. As an alternative to CDM, damage, which may ultimately lead to fracture, can be accounted for by so-called fracture criteria, which predict fracture in terms of the accumulation of certain stress states. Chen et al. [1] investigated cold extrusion processes with those fracture criteria.

The goal of this work is the analysis of a cold extrusion process for 16MnCr5 in terms of damage and the comparison of different damage and fracture formulations. The material and model parameters associated with the constitutive damage model and the fracture criteria are determined by an inverse parameter identification process for notched tensile tests. Since no macroscopic cracks occur for the experimental setups of the cold extrusion processes investigated in this work, the predictions for damage are validated by comparison with scanning electron microscopy images of voids.

2 FRACTURE AND DAMAGE MODELING

In general, the prediction of damage with fracture criteria is based on very little information about the material and stress states, resulting in a low effort for the computation and the implementation. These criteria can be either used coupled or uncoupled to the FE analysis. While softening effects cannot be conducted, the criteria can be coupled to the simulation via element deletion. In this case, the interaction arises trough changes in stiffness. Although such failure criteria give an estimation of the damage, they do not cover any other effects that micro-cracks might have. Damage can decrease the elasticity modulus, the yield stress, the hardness, the ultrasonic waves velocity, the density or increase the electrical resistance. Constitutive models are capable of covering those effects, since the evolution of damage can be modelled more accurately. However, the computational cost compared to the fracture criteria is higher.

2.1 Fracture Criteria

Various fracture criteria exist to predict failure in forming processes. Most of them can be written as the integral of a function of the stress state expressed in terms of the Cauchy stress $f(\boldsymbol{\sigma})$ over the plastic equivalent strain α with the failure strain α_f as the upper boundary, i.e.

$$C = \int_0^{\alpha_\mathrm{f}} f(\boldsymbol{\sigma})\, d\alpha \ . \tag{1}$$

The variable C can be interpreted as the critical value when failure occurs and therefore is a material parameter.

The established models of Freudenthal, Cockcroft and Latham and Oyane are implemented in this work and explained in the following.

According to Freudenthal [4], the critical parameter at fracture

$$C_{\mathrm{F}} = \int_0^{\alpha_{\mathrm{f}}} \sigma_{\mathrm{eq}} \, d\alpha \ , \tag{2}$$

is a measure for the absorbed energy per unit volume, where σ_{eq} denotes the equivalent stress. This model does not consider the effect of high tensile stresses or hydrostatic stress states explicitly.

Cockcroft and Latham [2] postulated that fracture is triggered by the maximum principle tensile stress instead of the generalized stress. Therefore, the critical material dependent value at fracture

$$C_{\mathrm{CL}} = \int_0^{\alpha_{\mathrm{f}}} \langle \sigma_{\mathrm{p},1} \rangle \, d\alpha \tag{3}$$

is defined as the integral over the largest positive principal stress. The first principal stress is denoted by $\sigma_{\mathrm{p},1}$, where $\sigma_{\mathrm{p},i}$ represents the i-th principal stress, with $\sigma_{\mathrm{p},1} \geq \sigma_{\mathrm{p},2} \geq \sigma_{\mathrm{p},3}$. The expression $\langle \bullet \rangle$ represents the Macaulay brackets, i.e. $\langle \bullet \rangle = 0, \quad \forall \bullet < 0$ and $\langle \bullet \rangle = \bullet, \quad \forall \bullet \geq 0$. This criterion does not consider the influence of hydrostatic stresses explicitly.

Oyane et al. [10] consider a void growth model. They postulate

$$C_{\mathrm{O}} = \int_0^{\alpha_{\mathrm{f}}} \left[1 + \frac{1}{a_0} \frac{\sigma_{\mathrm{h}}}{\sigma_{\mathrm{eq}}} \right] d\alpha \tag{4}$$

to be the criterion for fracture, where $\sigma_{\mathrm{h}} = \frac{1}{3} \mathrm{tr}(\boldsymbol{\sigma})$ denotes the hydrostatic stress. The parameter a_0 can be adapted inside reasonable limits for a better correlation of numerical and experimental results. It is connected with the volumetric strain and can be derived by experiments with two different stress states, as explained in [10].

2.2 Continuum Damage Model

An elasto-plastic material model coupled with damage is selected for this article. It is based on the work of Lemaitre, see [8], with modifications following the implementation of Soyarslan et al. [13, 14]. All simulations in this work are performed with the commercial FE software Abaqus. In the following, the constitutive model is introduced as it is implemented in the framework of the Fortran-based user subroutines for finite strains. It is formulated in terms of the rate of the Mandel stresses and logarithmic stretches.

To define damage, the variable D, with $D \in [0,1]$, is introduced, which describes the surface density of mechanical defects. The stresses acting on the resisting area are called effective stresses, with $\tilde{\bullet} = \bullet/[1-D]$, where $\bullet$ can be any stress measure.

The deformation gradient

$$\boldsymbol{F} = \boldsymbol{F}^{\mathrm{e}} \cdot \boldsymbol{F}^{\mathrm{p}} \tag{5}$$

is decomposed multiplicatively into elastic and plastic parts, $\boldsymbol{F}^{\mathrm{e}}$ and $\boldsymbol{F}^{\mathrm{p}}$, respectively, see [7]. Using the polar decomposition theorem, the deformation gradient can be written as

$$\boldsymbol{F} = \boldsymbol{R} \cdot \boldsymbol{U} = \boldsymbol{V} \cdot \boldsymbol{R} \ , \tag{6}$$

where $\boldsymbol{R}$ is an orthogonal rotation tensor and $\boldsymbol{U}$ and $\boldsymbol{V}$ are symmetric deformation tensors, representing the stretches, as explained in [3]. The logarithmic stretches

$$\ln(\boldsymbol{U}) = \ln(\boldsymbol{U}^{\mathrm{e}}) + \ln(\boldsymbol{U}^{\mathrm{p}}) \tag{7}$$

can be decomposed additively into the elastic $\ln(\boldsymbol{U}^{\mathrm{e}})$ and plastic $\ln(\boldsymbol{U}^{\mathrm{p}})$ part. The rate of the elastic logarithmic strecth $\overline{\ln(\dot{\boldsymbol{U}}^{\mathrm{e}})}$ can be approximated as

$$\overline{\ln(\dot{\boldsymbol{U}}^{\mathrm{e}})} = \boldsymbol{R}^{\mathrm{e}^T} \cdot \boldsymbol{D} \cdot \boldsymbol{R}^{\mathrm{e}} - \boldsymbol{D}^{\mathrm{p}} \tag{8}$$

for small elastic strains ($|\boldsymbol{U}^{\mathrm{e}}| \ll 1$). Assuming that the plastic spin $\boldsymbol{W}^{\mathrm{p}} = \mathrm{skw}(\boldsymbol{L}^{\mathrm{p}}) \approx \boldsymbol{0}$ in terms of the plastic part of the velocity gradient $\boldsymbol{L}^{\mathrm{p}} = \dot{\boldsymbol{F}}^{\mathrm{p}} \cdot \boldsymbol{F}^{p-1}$ can be neglected, one obtains

$$\dot{\boldsymbol{R}}^{\mathrm{e}} = \boldsymbol{W} \cdot \boldsymbol{R}^{\mathrm{e}} - \boldsymbol{R}^{\mathrm{e}} \cdot \boldsymbol{W}^{\mathrm{p}} \tag{9}$$

for the elastic rotation. With this at hand, the rate of the effective Mandel stresses is defined as

$$\dot{\tilde{\boldsymbol{M}}} = \lambda_0 \, \mathrm{tr}(\overline{\ln(\dot{\boldsymbol{U}}^{\mathrm{e}})}) \, \boldsymbol{I} + 2 \, \mu_0 \, \overline{\ln(\dot{\boldsymbol{U}}^{\mathrm{e}})} \ , \tag{10}$$

where the Mandel stresses are related to Cauchy stresses via

$$\boldsymbol{\sigma} = \frac{\boldsymbol{R}^{\mathrm{e}} \cdot \boldsymbol{M} \cdot \boldsymbol{R}^{\mathrm{e}^T}}{\det(\boldsymbol{F})} \ . \tag{11}$$

The damage associated driving force, also referred to as energy density release rate

$$Y = \frac{1+\nu}{2\,E} \left[\langle \tilde{\boldsymbol{M}} \rangle^{+} : \langle \tilde{\boldsymbol{M}} \rangle^{+} + h \, \langle \tilde{\boldsymbol{M}} \rangle^{-} : \langle \tilde{\boldsymbol{M}} \rangle^{-} \right] - \frac{\nu}{2\,E} \left[\left\langle \mathrm{tr}(\tilde{\boldsymbol{M}}) \right\rangle^{2} + h \, \langle \mathrm{tr}(-\tilde{\boldsymbol{M}}) \rangle^{2} \right] \tag{12}$$

is defined as proposed by Soyarslan et al. [13, 14]. The variable h was introduced by Lemaitre as a material-dependent parameter associated with closing micro-defects. In the latter definition of the damage related driving force, the crack-closure effect is not taken into account. Here, h controls the delayed void growth under compressional loading.

The hardening law is chosen to be of a Swift-type, see [15], which defines the yield stress as

$$q = A \, [\alpha_0 + \alpha]^n \ , \tag{13}$$

where A, α_0 and n are material parameters. The yield function is defined as

$$\Phi^{\mathrm{y}}(\boldsymbol{M}, q, D) = \tilde{M}_{\mathrm{eq}} - q \ , \tag{14}$$

with $\tilde{M}_{\mathrm{eq}} = \sqrt{(\tilde{\boldsymbol{M}} : \mathbb{H} : \tilde{\boldsymbol{M}})}$, where $\mathbb{H}$ is the the so-called Hill-operator [5]. With this at hand, the plastic part of the deformation rate can be derived as

$$\boldsymbol{D}^{\mathrm{p}} = \dot{\lambda} \frac{\partial \Phi}{\partial \boldsymbol{M}} = \dot{\lambda} \frac{1}{1-D} \frac{\mathbb{H} : \tilde{\boldsymbol{M}}}{\tilde{\boldsymbol{M}}_{\mathrm{eq}}} \ , \tag{15}$$

where $\dot{\lambda}$ represents the plastic multiplier. The evolution of damage is given via the relation

$$\dot{D} = \dot{\lambda} \left\langle \frac{Y - Y_0}{S} \right\rangle^{\kappa} \frac{1}{[1-D]^{\beta}} \ , \tag{16}$$

where κ, S, Y_0 and β are material parameters.

3 Parameter Identification Process

Material models and fracture criteria used for the simulation of forming processes are generally based on a variety of material and model parameters. For the mathematical modeling of complex material behaviours, adapting the model parameters is essential for the accurate prediction of the material response. While some parameters like the Young's modulus and the Poisson's ratio can be computed directly, others can not. A common approach is an inverse parameter identification process. The aim of the inverse problem of parameter identification is to minimize the deviation between the experimental data and the data obtained by numerical simulations using an optimal set of parameters, under the consideration of mathematical and physical constraints.

To this end, a simulation of the experimental setup has to be performed multiple times, where the material parameters are iteratively updated, until the numerical and experimental results match as best as possible. Mathematically speaking, the optimal parameter set is defined by the minimization problem of the form

$$\min_{\boldsymbol{\kappa}} \left(f(\boldsymbol{\kappa}) \right), \ \forall \, \boldsymbol{\kappa} \in \boldsymbol{K}, \ \text{with } \boldsymbol{K} = \{ \boldsymbol{\kappa} \,|\, \boldsymbol{h}(\boldsymbol{\kappa}) = \boldsymbol{0}, \ \boldsymbol{g}(\boldsymbol{\kappa}) \leq 0 \} \ . \tag{17}$$

where $f(\boldsymbol{\kappa})$ is the objective or error function. It depends on the parameter set $\boldsymbol{\kappa}$ which underlies equality $\boldsymbol{h}$ and inequality constraints $\boldsymbol{g}$.

While the simulations of the experiments are performed with Abaqus, the algorithm for the parameter identification process is implemented in Python, making use of the provided optimization library. Since the minimization algorithms do not necessarily find global minima, all parameter identification processes have been performed with various initial guesses for the starting parameter vectors and different optimization algorithms, i.e. zero-order and gradient-based methods as well as evolutionary algorithms.

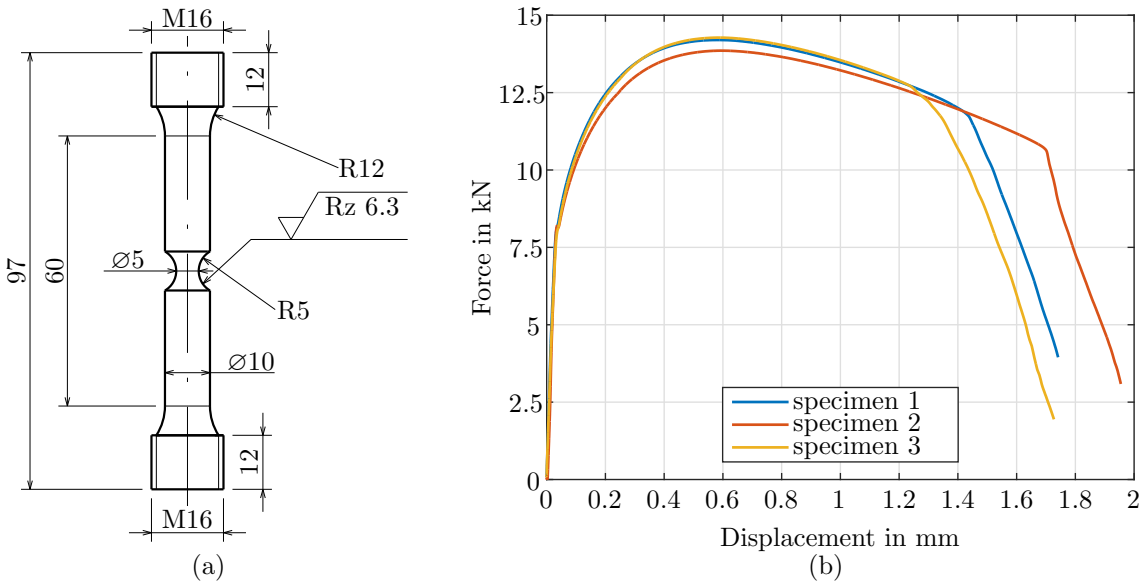

Figure 1: Engineering drawing of the specimen (a) and load displacement curves obtained from the experiments (b).

In general, it is possible to compare any values of the simulation with the experimental data. In this work, the optimization procedure is always applied to the full body response, i.e. the load displacement curve. To this end, the objective function is defined as

$$f(\boldsymbol{\kappa}) := \sqrt{\sum_{i=1}^{n_{\mathrm{sp}}} \left[\boldsymbol{w}(i) \ \left[\boldsymbol{f}^{\mathrm{sim}}(\boldsymbol{\kappa}, i) - \boldsymbol{f}^{\mathrm{exp}}(i)\right]\right]^2} \,, \tag{18}$$

which is a least-square-like error function, where i denotes the summation index, with $i \in n_{\mathrm{sp}}$ and n_{sp} represents the number of sample points. It measures the difference between the numerically and experimentally obtained reaction forces $\boldsymbol{f}^{\mathrm{exp}}$ and $\boldsymbol{f}^{\mathrm{sim}}$, respectively, weighted by $\boldsymbol{w}$.

To this end, experiments have to be carried out in order to generate data for comparison to the simulation results. Notched tensile tests are performed to induce a localization of the deformation and to impose an inhomogeneous stress field throughout the entire experiment. The resulting load displacement curves, as depicted in Figure 1(b), show variations in curvature, as well as differences in the point of crack initiation and failure. Since the response of specimen 1 yields an average behaviour, the following parameter identification processes are performed with respect to its associated experimental data.

Since isotropy is considered, the parameters associated with the Hill operator are chosen as $r_0 = r_{45} = r_{90} = 1$. The elastic properties, i.e. the Young's modulus and the Poisson's ratio, are determined analytically as $E = 210000$ MPa and $\nu = 0.3$, see [11].

Table 1: Identified parameters for elasto-plastic continuum model in conjunction with fracture criteria.

A	9.332	$\cdot 10^{2}$	MPa
α_0	1.196	$\cdot 10^{-3}$	
n	1.575	$\cdot 10^{-1}$	
C_{CL}	5.912	$\cdot 10^{2}$	MPa
C_{F}	4.069	$\cdot 10^{2}$	MPa
C_{O}	9.859	$\cdot 10^{-1}$	

Table 2: Identified parameters for fully coupled continuum model.

A	1.043	$\cdot 10^{3}$	MPa
α_0	5.630	$\cdot 10^{-3}$	
n	2.095	$\cdot 10^{-1}$	
κ	3.087	$\cdot 10^{0}$	
S	3.226	$\cdot 10^{0}$	MPa
Y_0	3.710	$\cdot 10^{-2}$	MPa
β	1.989	$\cdot 10^{1}$	
D_{crit}	4.607	$\cdot 10^{-1}$	

3.1 FE-Model for the Notched Tensile Test

The FE-model including the geometry, the mesh and the boundary conditions of the notched tensile test is shown in Figure 2(a). Axisymmetry, as well as symmetry with respect to the horizontal plane is considered. The geometry is discretized with 230 four-noded, axisymmetric, quadrilateral elements with reduced integration (type CAX4R) and an edge length of 4.3 mm. The load is applied linearly over time as displacement boundary conditions on the thread. In the experiment, the displacements were tracked with an extensometer, with its sensors positioned 20 mm above and below the plane of horizontal symmetry, as indicated in Figure 2(a). The displacements are evaluated at a node at the same exact position to reproduce the load displacement curve correctly.

For the depiction of cracks in FE analyses, element deletion is used. To this end, the parameter D_{crit} is introduced as a threshold value to trigger the removal of elements. The simulations are performed with Abaqus/Explicit.

3.2 Identification of Plasticity Parameters

In this section, a parameter identification is performed for elasto-plasticity with Swift-type hardening, as introduced in Section 2.2. To this end, the error in the load displacement curves in the elasto-plastic area, which is the region before the crack starts to develop, is minimized.

The associated load displacement curve is depicted in Figure 2(b). The numerical results for the optimized parameter set, as shown in Table 1, are in good agreement with the experimental data.

3.3 Parameter Identification for the Fracture Criteria

In the following, an identification of the parameters for the fracture criteria, i.e. $C_{\mathrm{F}}, C_{\mathrm{CL}}$ and C_{O}, as shown in eqs. (3) to (4), is carried out. These constants are used as threshold values for material failure and therefore trigger element deletion. The fracture criteria are used in conjunction with a Swift-type hardening model with the optimized parameter set identified in the previous section.

Performing the test, the specimen fully fails immediately after crack initiation. Since there is no material softening, an excessive amount of elastic energy is released upon

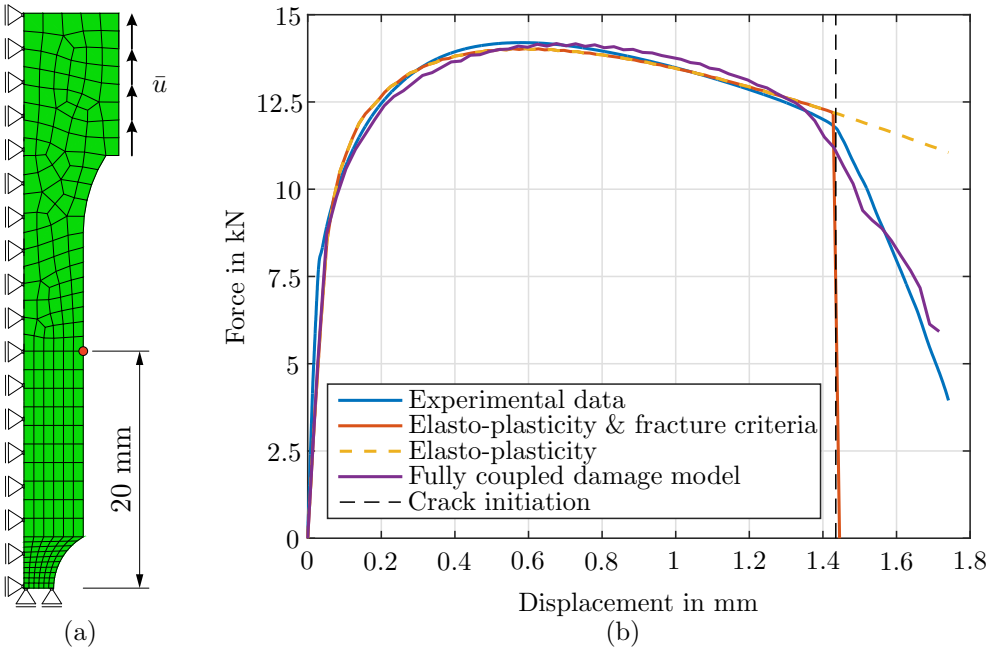

Figure 2: Illustration of the FE-model of the notched tensile test (a). The node, where the displacement is recorded for the load displacement curves, is marked by the red dot. The load displacement curves of the experiment and the simulations (b) are performed with optimized parameter sets.

failure, resulting in unrealistic large vibrations. The resulting oscillations in reaction forces are removed for visualization purposes. Since the time discretization is identical for all simulations, the resulting load displacement curves are identical for all fracture criteria, as depicted in Figure 2(b). The identified threshold values are shown in Table 1.

3.4 Parameter Identification for the Continuum Damage Model

In this section, a parameter identification process for the continuum damage model is performed. In general, various options exist to realize this. One way is the identification of only the damage related parameters, based on the optimized plasticity, as done in Section 3.2. The load displacement curve does not hold any information about the initiation of the damaging process, because the decrease in the reaction force does not necessarily has to be damage induced and can be caused solely by cross section reduction of the specimen. Thus, the optimization of the plasticity and damage associated parameters simultaneously could be another possible way for performing the parameter identification process. This implies, that the damage evolution can start at basically any point.

Here, the latter approach is implemented, because it is more reasonable that the damage evolution is a steady process, that most likely occurs before the crack initiation on macroscopic scale. Since the stress state is purely tensional, the parameter h has no influence on the results and has to be obtained from different experiments. To this end, h

is set to zero.

The resulting load displacement curve is depicted in Figure 2(b). The numerical data is associated with the optimized parameter set in Table 2. While the specimen fails immediately after crack initiation using the fracture criteria, a developing crack can be observed for the continuum damage model.

4 SIMULATION AND ANALYSIS OF COLD EXTRUSION PROCESSES

In the following, the simulation of a cold extrusion process is presented, based on the parameter sets identified in the previous sections.

Simulations are performed for two experimental setups with different extrusion strains, i.e. $\varphi_1 = 0.5$ and $\varphi_2 = 1.0$. The extrusion strain φ is defined as $\varphi = \ln(A_0/A_1)$, where A_0 and A_1 represent the cross sections before and after the extrusion, respectively. The initial workpiece diameter is $D_0 = 30$ mm. A friction coefficient of $\mu = 0.04$ between workpiece and die is used. The shoulder opening angle of the die is defined as $\alpha^* = 45°$, the transition radii are set to 3 mm and an undercut is used. For the sake of saving computational time, axisymmetry is considered for the FE model. The billet is discretized with 4260 four-noded, axisymmetric, quadrilateral elements with reduced integration (type CAX4R) with an edge length of 4.3 mm. The die is modeled as a linear-elastic solid with a Young's modulus of $E_{\text{die}} = 210000$ MPa and a Poisson's ratio of $\nu_{\text{die}} = 0.3$. The parameter sets identified in the previous sections are used. The workpiece is pushed trough the die by a constant velocity of 6.1 mm/s over 7.1 s of process time.

Figure 4 depicts the damage distribution for the continuum damage model for the two experimental setups. It can be observed that the maximum damage appears beneath the surface of the billet. The level of damage for the smaller extrusion strain φ_1 is higher on the central axis compared to φ_2, which is also observed in the experiments, as seen in Figure 4.

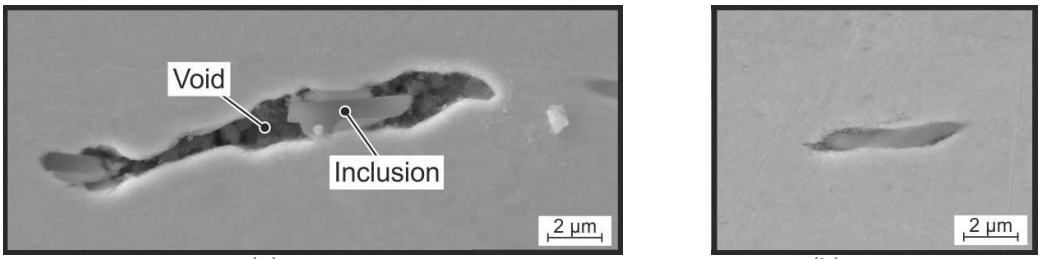

(a) $\varphi = 0.5$ (b) $\varphi = 1.0$

Figure 3: SEM micrographs of 16MnCr5 for extrusion strains of $\varphi = 0.5$ (a) and $\varphi = 1.0$ (b). Taken from [16].

The contour plots of damage for the fracture criteria are shown in Figure 5. Here, damage is defined by the actual value of the associated damage criterion $C_\bullet$ divided by the critical value $C_{\bullet,\text{crit}}$ identified in Section 3.3. Comparing all contour plots for φ_1, they show significant variations in values and distribution. While the maximum damage in the stationary region is 1.5 %, and therefore, rather low, the maximum damage for the criteria

of Cockcroft-Latham, Freudenthal and Oyane is 42 %, 292 % and 51 %, respectively. Using the criteria of Cockcroft-Latham and Oyane, most damage occurs in the center, while the criterion of Freudenthal predicts the highest damage beneath the surface.

Isik et al. investigated damage in terms of void volume fraction experimentally. It was shown that the damage in the dual phase steel DP600 was below 1 % for equivalent plastic strains of up to 0.8. Since 15MnCr6 shows a similar mechanical behavior to DP600, the results of the CDM model seem reasonable, while the damage predicted by the fracture criteria is significantly overestimated.

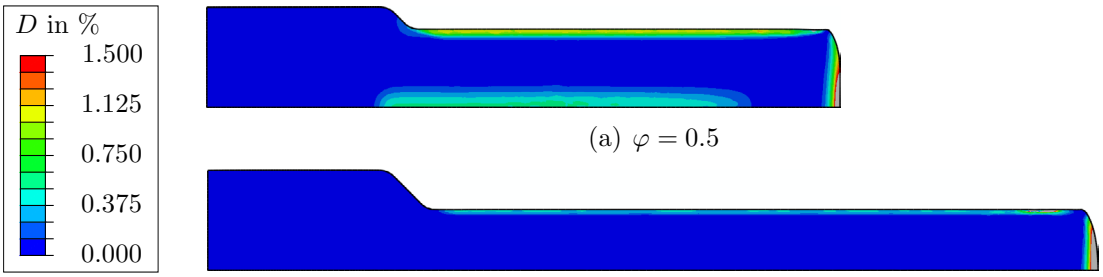

(a) $\varphi = 0.5$

(b) $\varphi = 1.0$

Figure 4: Contour plot of damage D distribution for cold extrusion for extrusion strains of $\varphi = 0.5$ (a) and $\varphi = 0.1$ (b) with the use of the continuum damage model.

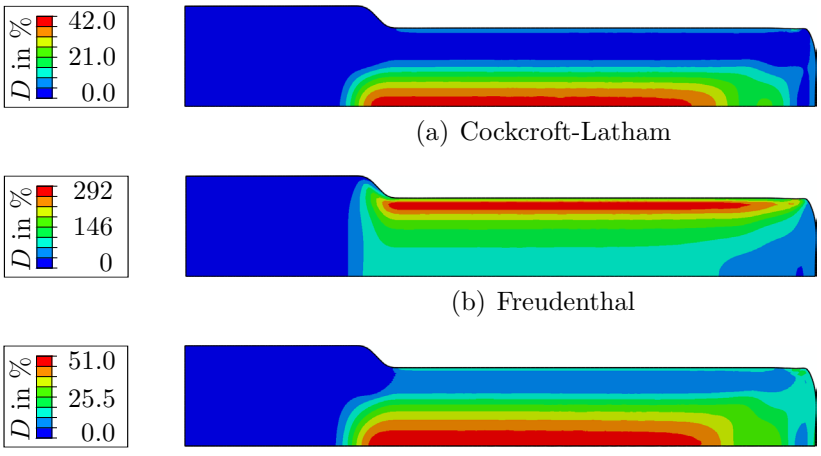

(a) Cockcroft-Latham

(b) Freudenthal

(c) Oyane

Figure 5: Contour plot of damage D distribution for the fracture criteria of Cockcroft-Latham (a), Freudenthal (b) and Oyane (c) for the cold extrusion process with φ_1. The damage value is defined by the actual value of the criterion, divided by the critical value identified in Section 3.3.

5 CONCLUSION

From the simulation results it can be concluded that the use of the presented fracture criteria is very limited and only reasonable in certain cases. In this work, the coupling

between the fracture criteria and the stresses is not implemented, so the effect of damage induced softening cannot be captured explicitly, leading to an overestimated stiffness. Fracture criteria depend on a single stress-dependent function and cannot distinguish between different damage mechanisms, which may lead to errors. Cracks can be depicted by coupling those fracture criteria to an element deletion criterion. Removing undamaged elements, however, is associated with the removal of energy and mass, which may influence the physical behavior. A fine discretization would diminish this effect, but is related to increasing computational effort.

A CDM model generally yields a better prediction of the damage, up to the point of fracture. Elasticity is coupled to the damage evolution and therefore the effect of damage induced softening can be captured. Here, the removal of elements with damaged material is not as significant as for the fracture criteria due to the decrease in stiffness. The CDM model presented in this work can be adapted to the problem more accurately, since the evolution of damage is controlled by several parameters. While the fracture criteria only depend on a single stress dependent function, the constitutive damage model can distinguish between different stress states.

ACKNOWLEDGEMENT

Funding of project S01 within the Collaborative Research Centre CRC/Transregio 188 "Damage-controlled forming processes" by the German Research Foundation (DFG) is highly acknowledged.

REFERENCES

[1] D.C. Chen, S.K. Syu, C.H. Wu, S.K. Lin, Investigation into cold extrusion of aluminum billets using three-dimensional finite element method, Journal of Materials Processing Technology 192-193, pp. 188-193, 2007.

[2] M.G. Cockcroft, D.J. Latham. Ductility and the Workability of Metals, Journal of the Institute of Metals, 96, pp. 33-39, 1968.

[3] F. Dunne, N. Petrinic. Introduction to computational plasticity, Oxford: Oxford University Press, 2005.

[4] A.M. Freudenthal. The inelastic behaviour of engineering materials and structures, Wiley, New York, 1950.

[5] R. Hill. A theory of the yielding and plastic flow of anisotropic metals. Proceedings of the Royal Society of London, 1948.

[6] K. Isik, G. Gerstein, T. Clausmeyer, F. Nürnberger, A.E. Tekkaya, H.J. Maier, Evaluation of Void Nucleation and Development during Plastic Deformation of Dual-Phase Steel DP600. Steel research int. 87, No. 9999, 2016.

[7] E. Lee. Elastic-Plastic Deformation at Finite Strains. ASME. J. Appl. Mech 36(1):1-6, 1969.

[8] J. Lemaitre, R. Desmorat. Engineering Damage Mechanics. Springer, 2005.

[9] C. McVeigh, W.K. Liu. Prediction of central bursting during axisymmetric cold extrusion of a metal alloy containing particles, International Journal of Solids and Structures 43, pp. 3087-3105, 2006.

[10] M. Oyane, T. Sato, K. Okimoto. Criteria for ductile fracture and their applications, Journal of Mechanical Working Technology 4, pp. 65-81, 1980.

[11] F. Richter. The 100 Steels Programme (https://www.tugraz.at/fileadmin/user_upload/Institute/IEP/Thermophysics_Group/Files/Staehle-Richter.pdf).

[12] K. Saanouni, J.F. Mariage, A. Cherouat, P. Lestriez. Numerical prediction of discontinuous central bursting in axissymmetric forward extrusion by continuum damage mechanics, Computers and Structures 82, pp. 2309-2332, 2004.

[13] C. Soyarslan, A.E. Tekkaya. U. Akyuz, Application of Continuum Damage Mechanics in discontinuous crack formation: Forward extrusion chevron predictions, ZAMM - Journal of Applied Mathematics and Mechanics, Volume 88, Issue 6, pp. 436-453. WILEY-VHC, 2008.

[14] C. Soyarslan, A.E. Tekkaya. Finite deformation plasticity coupled with isotropic damage: Formulation in principal axes and applications, Finite Elements in Analysis and Design archive, Volume 46, Issue 8, pp. 668-683, 2010.

[15] H. W. Swift. Plastic instability under plane stress. Journal of the Mechanics and Physics of Solids 1, pp. 1-18, 1952.

[16] A.E. Tekkaya, N. Ben Khalifa, O. Hering, R. Meya, S. Myslicki, F. Walther. Forming-induced damage and its effects on product properties, CIRP Annals Manufacturing Technology, accepted for publication 2017.